Scaling analysis of narrow necks in curvature models of fluid lipid-bilayer vesicles

Bertrand Fourcade,* Ling Miao,† Madan Rao,‡ and Michael Wortis
Department of Physics, Simon Fraser University, Burnaby, British Columbia, Canada V5A 1S6

R. K. P. Zia
Department of Physics and Center for Stochastic Processes in Science and Engineering, Virginia Polytechnic Institute and State University, Blacksburg, Virginia 24061-0435
(Received 8 November 1993)

Under appropriate conditions fluid lipid-bilayer vesicles in aqueous solution take the form of two (or more) compact shapes connected by a narrow neck (or necks). We study the limit (termed "vesiculation") in which the neck radius a approaches zero. On the basis of elastic equations, derived originally by Deuling and Helfrich [J. Phys. (Paris) **37**, 1335 (1976)] for a bending-energy model (the spontaneous-curvature model), we show analytically that, at vesiculation, the local curvatures of the two regions joined by the neck satisfy a simple, universal "kissing" (osculation) condition. Furthermore, for points near but not at the vesiculation limit, a is small but nonzero and there is characteristic scaling behavior. For example, in the surface tension (σ) and pressure (p) variables, the vesiculation boundary is a line in the (σ,p) plane, and the quantity $a \ln a$ scales linearly with the distance $(\Delta\sigma,\Delta p)$ from the boundary. These relations have been observed numerically, but no analytic discussion has previously appeared in the literature. Results for the spontaneous-curvature model generalize easily to other (more physical) bending-energy models.

PACS number(s): 82.70.−y, 87.22.Bt, 68.15.+e, 68.60.Bs

I. INTRODUCTION: BUDDING AND VESICULATION, NECKS AND MULTIPLETS

Previous theoretical work by our group [1] and others [2–6] has shown that, under appropriate conditions, the equilibrium configuration of a fluid vesicle of spherical topology with fixed volume and area may take the form of two (or more) compact bodies connected by a narrow neck (or necks). Such shapes are, indeed, observed in the laboratory [3,6–10]. Two generically different situations are possible. In the first, called budding or necking, the neck has a positive radius a and the entire shape including the constriction satisfies a Euler equation which results from constrained minimization of the total bending energy. In the second, called vesiculation, the neck has become infinitesimal and the stable state corresponds to a boundary minimum in the space of configurations. Here, the shape of the neck is not well defined [11] (in particular, it does not satisfy a Euler equation), and the minimum-energy configuration consists of a "multiplet" of separate Euler shapes [1], touching one another tangentially (i.e., osculating) and possessing, collectively, the required total area and volume. At particular points in the (shape) phase diagram, changing a control parameter (area, volume, spontaneous curvature, or their Legendre conjugates) allows one to pass smoothly between necked and vesiculated shapes. We call this behavior a "kissing transition," since it marks the boundary between osculating and nonosculating shapes.

At first sight, it may appear surprising that necked and vesiculated shapes can correspond to energy minima, since curvatures in such regions are large and might be expected to produce high bending energies. In fact, what happens in the neck region is that one principal curvature becomes large and positive, while the other becomes large and negative in just such a way that the mean curvature, which controls the bending energy, remains closely matched to the spontaneous curvature. The contribution of the neck region to the total energy in fact vanishes as the neck radius goes to zero. This cancellation requires a delicate adjustment of the vesicle shape in the neck region.

It is the purpose of this paper to study analytically vesicle shapes at and near the kissing transition. The kissing transition is second order, in the sense that first derivatives of the total bending energy with respect to the control parameters are continuous. Near the transition, shapes involving mechanically equilibrated narrow necks are very close in overall energy to similarly shaped multiplets. The mathematical mechanism for the transition is a (nonstandard) bifurcation [12]. The Landau function for a normal pitchfork bifurcation involves terms varying as φ^2 and φ^4, where φ is the order parameter. The princi-

*Permanent address: Maison des Magistères Jean Perrin, C.N.R.S., 25 Avenue des Martyrs, B. P. 166, 38042 Grenoble Cedex 9, France.
†Present address: Department of Biochemistry, McMaster University, 1200 Main Street West, Hamilton, Ontario, Canada L8N 3Z5.
‡Present address: Institute of Mathematical Sciences, C.I.T. Campus, Taramani, Madras 600 113, India.

pal control parameter is the coefficient of the φ^2 term, and the transition occurs when this parameter passes through zero. Here, the neck radius a will play the role of the order parameter; however, the important terms in the Landau function will be found to vary as a and $a^2 \ln a$, and the principal control parameter, which measures distance from the phase transition, is the coefficient of the linear term. Thus we shall find that the neck radius a and the energy splitting ΔE between necked and vesiculated configurations do vary with the control parameter in a characteristic scaling manner, but not with the usual critical exponents. Furthermore, as $a \to 0$, we shall find that the entire neck region has a simple shape on the scale of the small distance a. In addition, it turns out that at the transition there is a remarkably simple relation between the local radii of curvature at the point of contact,

$$1/R_1 + 1/R_2 = 2/R_0 \equiv c_0 , \tag{1}$$

where R_1 and R_2 are the radii of curvature at the opposite sides of the point of contact (we assume that the contact is axisymmetric), c_0 is the spontaneous curvature, and R_0 is the radius of the "Helfrich sphere," which has bending energy zero. The kissing condition (1) was already used in Ref. [1] to locate certain phase boundaries [13]. It has been observed numerically in a number of studies of vesicle shapes [1,3]. However, no analytic proof yet appears in the literature.

We phrase the discussion in the context of the spontaneous-curvature model, originally studied by Helfrich and Deuling [14,15], which attributes to the bilayer an intrinsic preference for a state of predetermined local mean curvature c_0; however, the results are applicable to other, more realistic bending-elasticity models of vesicle shape. The spontaneous-curvature model is probably not physically relevant in it simplest form and has been superseded by the area-difference (ΔA) model [3,4,16–20], which attributes the mean curvature preference to the difference in the number of lipid molecules in the two leaves of the bilayer, and, most recently, by the area-difference-elasticity (ADE) model [6,17–23], which includes the effect of lateral stress on the area difference. The key point is that all three models are closely related and share the same Euler equations, which express the appropriately constrained energy minimization required for mechanical equilibrium. Thus, in the ΔA model, the parameter c_0 is replaced in essence by the Lagrange multiplier [3,4] which fixes the area difference; while, in the ADE model, this Lagrange multiplier becomes self-consistently determined [21,23]. However, with these changes, all three models generate the same Euler (Helfrich) equations and, therefore, the same catalog of stationary shapes. It is convenient to do the narrow-neck analysis for the spontaneous-curvature model, which makes the notation simplest. The analysis is local in the sense that it looks only at a single free-energy branch, as that branch approaches its vesiculation threshold. In applying the results to the other models, one must only keep in mind that the following are model specific: (a) the meaning of the parameter c_0 and (b) the global question of which free-energy branch provides the shape of lowest mechanical energy.

Finally, we remark that the analysis done here is for the case of "exterior budding," where the bud is outside the parent vesicle, corresponding to the exocytotic geometry. An identical and equivalent analysis can be done for the case of "interior budding," corresponding to the endocytotic geometry.

The plan of this paper is as follows. Section II recapitulates the notation and equations of Ref. [1], insofar as they are needed here, including the energy functional and the corresponding axisymmetric Euler equation. Section III addresses in a heuristic way the question, "Can a small neck be a mechanically stable, low-energy configuration?" Although the argument here is variational, it will turn out that it captures many important features of the full solution, including the kissing condition (1). Section IV studies perturbative development of the axisymmetric shape equations about closed Euler shapes. This is relevant because a small deviation ϵ in initial curvature from that of a closed shape leads to a failure of closure at the opposite end, producing a narrow neck. Thus the neck radius $a \to 0$, as $\epsilon \to 0$. The calculation is carried out explicitly for perturbations of a spherical shape. Section V focuses in on the neck region and shows that, to leading order as $a \to 0$, the shape of the neck region is a "minimal surface," i.e., one whose mean curvature is everywhere zero. Corrections in powers of the neck radius a are developed systematically. Finally, in Sec. VI, we match the perturbative solution far from the neck to the scaling solution near the neck to derive the kissing condition for spherical shapes. The technique here is related to asymptotic matching and boundary-layer theory [24]. Section VII describes generalization to axisymmetric but nonspherical shapes. An Appendix contains some important details of perturbative shape calculations near a local extremum of the radius, such as a neck or belly.

II. FORMULATION AND NOTATION

To find the equilibrium vesicle shape for the spontaneous curvature model, it is necessary to minimize the Helfrich bending energy [14,25],

$$E[c_1,c_2;\mathcal{S}] = \frac{\kappa}{2} \oint dA\, [c_1(\mathbf{r}) + c_2(\mathbf{r}) - c_0]^2 , \tag{2}$$

at fixed surface area A and enclosed volume V. The integral is over the closed surface $\mathcal{S}$. The quantities $c_i(\mathbf{r}), i = 1,2$, are the local principal curvatures at the point $\mathbf{r}$ of $\mathcal{S}$. A term involving the Gaussian curvature has been omitted, since it is a topological invariant and we shall deal here with shapes of fixed (spherical) topology. In what follows, we choose length and energy scales such that the bending rigidity κ and the spontaneous curvature c_0 are made equal to unity. Incorporating the constraints in the usual way leads to the requirement that the free-energy functional,

$$\Phi[\mathcal{S}] = E[\mathcal{S}] - pV[\mathcal{S}] + \sigma A[\mathcal{S}] , \tag{3}$$

be made stationary with respect to variations of $\mathcal{S}$. The Lagrange multipliers [26] σ and p are then adjusted to achieve the desired A and V. Under the added restriction

of axisymmetry [27], this leads to equations [15] for the principal curvatures $c_m(r)$ and $c_p(r)$,

$$\frac{dc_m}{dr}+\frac{c_m-c_p}{r}=\frac{r}{2[1-(rc_p)^2]} \times\{c_p[(c_p-1)^2-c_m^2]+2\sigma c_p-p\} \quad (4)$$

and

$$\frac{dc_p}{dr}=\frac{c_m-c_p}{r}\ , \quad (5)$$

where r is the distance from the rotation axis. It will be useful in the following also to introduce (see Fig. 1) an arc length s measured from the origin and the angle Θ between the tangent to the shape and the normal to the symmetry axis, so

$$ds=\frac{dr}{\cos\Theta}=\frac{dz}{\sin\Theta}\ , \quad (6)$$

$$\frac{dz}{dr}=\tan\Theta\ , \quad (7)$$

$$c_p=\frac{\sin\Theta}{r}\ , \quad (8)$$

and

$$c_m=\frac{d\Theta}{ds}=\frac{d\sin\Theta}{dr}\ . \quad (9)$$

Imagine integrating Eqs. (4) and (5), starting at the origin with an initial curvature [28] $c_i=c_m(s=0)=c_p(s=0)$. In general, the shape will not close; however, generically there exists a discrete set of initial curvature values for which closure occurs. Suppose that c_i^* is a member of this set, so that the shape closes at some $s=s_f$ with a final axial curvature $c_f^*=c_m(s=s_f)=c_p(s=s_f)$, as shown in Fig. 1. Now, when c_i is very close to c_i^*, the integration will follow closely the curve of Fig. 1 up to the near vicinity of the axis, where it will deviate to form a narrow neck, as illustrated in Fig. 2. Note that the neck radius a depends upon (and goes to zero with) the small difference $\epsilon=c_i-c_i^*$. The two characteristic deviated shapes correspond to the two signs of ϵ. Of the two, Fig. 2(c) (nodoid) describes a self-intersecting surface and is forbidden for real vesicle [29]; while Fig. 2(a) (onduloid) describes a narrow, physically acceptable neck.

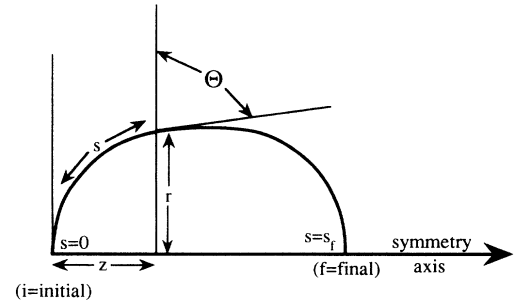

FIG. 1. Typical closed axisymmetric shape, illustrating the definition of variables. The Helfrich equations are integrated from the left, where the shape starts at the axis ($r=s=z=0$). The equations are singular at the axis, and, to get a smooth shape, it is necessary to start with $c_m=c_p=c_i$ at $s=0$. If c_i is chosen at an appropriate initial value $c_i=c_i^*$, then the shape closes at $s=s_f$ with $c_m=c_p=c_f^*$.

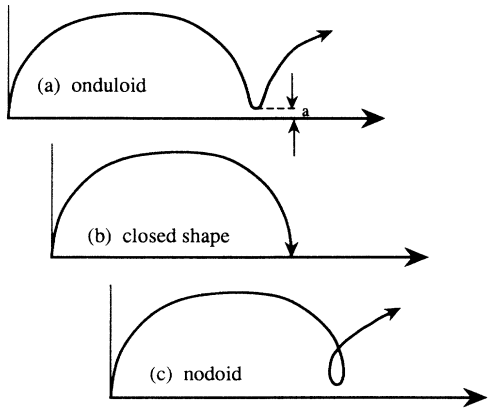

FIG. 2. Typical shapes which result from integrating the Helfrich equations when c_i is near c_i^*. When $c_i=c_i^*$, the shape closes as in (b). When $\epsilon\equiv c_i-c_i^*>0$, then integration leads to either the onduloid (a) or the nodoid (c). When $\epsilon\equiv c_i-c_i^*<0$, then (a) $\leftrightarrow$ (c). Whether it is the nodoid or the onduloid which corresponds to $\epsilon>0$ depends on the particular closed shape in question.

From this perspective, we can now give a generic description of the transition: If in the case of Fig. 2(a) further integration closes the shape, then the resulting vesicle is necked. The fact that this necked vesicle satisfies the Euler equation means that it is at mechanical equilibrium; however, the equilibrium may be either locally stable or locally unstable. A locally stable state may (or may not) correspond to a global energy minimum; a locally unstable state cannot. (In subsequent sections, we shall explore this question of stability in detail.) At a fixed $\epsilon\neq 0$ we cannot, generically speaking, expect closure; however, by varying ϵ we may expect to find a closed shape at some nonzero value $\epsilon=\epsilon(\sigma,p)$. By varying the control parameters σ and p, we shall find that it is possible to bring $\epsilon(\sigma,p)$ to zero. The condition $\epsilon(\sigma,p)=0$ defines a boundary in the (σ,p) plane [and, correspondingly, in the (A,V) plane]. On one side of this line, there is a closed nodoid shape; on the other side, there is a closed onduloid shape [30]. The limiting shape at the boundary is a multiplet (Fig. 2), which satisfies the kissing condition (1). This kissing multiplet lies on a multiplet free-energy sheet [1], which competes in energy with the free-energy sheet (or sheets) corresponding to the simple Euler shapes. On one side of the boundary, the Euler shapes have lower energy at fixed area and volume; on the other side, the multiplets have lower energy. Thus, when not preempted by another lower-lying sheet, the line $\epsilon(\sigma,p)=0$ is a kissing boundary.

In what follows, we shall compute in detail from Eqs. (2), (4), and (5) the shape of the narrow neck and the way in which the energy sheets for the Euler shape and the multiplet intersect along the kissing boundary. First,

however, it will be useful to present a simple variational calculation which captures much of the physics.

III. A TOY MODEL FOR NARROW NECKS

To find approximate solutions to the variational problem (2) imagine inserting into Eq. (3) a parametrized shape $\mathcal{S}$. If $\mathcal{S}$ has been judiciously chosen, then variation of the parameters can lead to a good representation of the full solution and, therefore, to a good approximation to the constrained minimum of Eq. (2). For example, choosing for $\mathcal{S}$ a sphere of radius R [corresponding to $\sin\Theta = r/R$ in Eqs. (8) and (9)] gives

$$\Phi[\mathcal{S}] \equiv \Phi_0(R) = 2\pi(2-R)^2 + 4\pi R^2\sigma - \tfrac{4}{3}\pi R^3 p \ . \quad (10)$$

Making $\Phi_0(R)$ stationary with respect to the parameter R then leads to

$$p = \frac{2\sigma+1}{R} - \frac{2}{R^2} \ , \quad (11)$$

which provides, in fact, the exact equilibrium radii [1],

$$R_\pm(\sigma,p) = [(2\sigma+1) \pm \sqrt{(2\sigma+1)^2 - 8p}\,]/2p \ , \quad (12)$$

for the two possible spherical solutions of Eqs. (4) and (5) compatible with given values of σ and p. Note [1] that $R_\pm(\sigma,p)$ are real provided $p < (2\sigma+1)^2/8$ and, within this region, both are positive when $p > 0$ and $\sigma > -\frac{1}{2}$.

To look at the problem of a narrow neck of radius a between two spheres of unequal radii R_1 and R_2, we adopt a trial shape [31] $\mathcal{S}$ (see Fig. 3) in which the two end caps (regions I and IV) are spherical but the inner regions (II and III) are described by [32]

$$\sin\Theta = \frac{1}{R_i + a}\left[r + \frac{R_i a}{r} \right] , \quad i = 1,2 \ , \quad (13)$$

which is chosen to fit the caps at the equators and to meet at the center in a neck of radius a. Note that $\sin\Theta(r)$ is continuous at the boundaries between regions [33]. The variational functional $\Phi[\mathcal{S}]$ is now parametrized by the three variables R_1, R_2, and a. The contributions from the end-cap regions I and IV are trivial. A brief calculation for region II gives, for the volume, area, and energy,

$$V_{\rm II}(R_1,a) = \frac{\pi R_1^3}{3}[(2+3p_1+2p_1^2)E(q_1) - 3p_1^2 K(q_1)] \ , \quad (14)$$

$$A_{\rm II}(R_1,a) = 2\pi R_1^2(1+p_1)E(q_1) \ , \quad (15)$$

and

$$E_{\rm II}(R_1,a) = \frac{1}{2}\left[\frac{2}{R_1+a} - 1 \right]^2 A_{\rm II}(R_1,a) \ , \quad (16)$$

where $p_i \equiv a/R_i$, $q_i \equiv \sqrt{1-p_i^2}$, $i = 1,2$, and the functions $E(q)$ and $K(q)$ are complete elliptic integrals [34]. Expanding the elliptic integrals for small a leads to the expressions,

$$V_{\rm I+II}(R_1,a) = \frac{4\pi R_1^3}{3} + \pi a R_1^2 + O(a^2) \ , \quad (17)$$

$$A_{\rm I+II}(R_1,a) = 4\pi R_1^2 + 2\pi a R_1 - \pi a^2 \ln(a/R_1) + O(a^2) \ , \quad (18)$$

and

$$E_{\rm I+II}(R_1,a) = 2\pi(2-R_1)^2 + \pi a[R_1 - 4/R_1] - \pi a^2 \ln(a/R_1)[(1-2/R_1)^2/2] + O(a^2) \ . \quad (19)$$

Equivalent expressions for region III+IV are obtained by replacing R_1 by R_2, so we may finally form the variational function corresponding to the trial shape of Fig. 3,

$$\Phi(R_1,R_2,a) = \Phi_0(R_1) + \Phi_0(R_2) + C(\sigma,p,R_1,R_2)\pi a - D(\sigma,p,R_1,R_2)\pi a^2 \ln a + O(a^2) \ , \quad (20)$$

where the coefficients of the terms in a and $a^2 \ln a$ are

$$C(\sigma,p,R_1,R_2) = (2\sigma+1)(R_1+R_2) - p(R_1^2+R_2^2) - 4(1/R_1 + 1/R_2) \quad (21)$$

and

$$D(\sigma,p,R_1,R_2) = (2\sigma+1) - 2\left[\frac{1}{R_1} + \frac{1}{R_2} \right] + 2\left[\frac{1}{R_1^2} + \frac{1}{R_2^2} \right] \quad (22)$$

and all higher-order terms have been dropped.

We now study the behavior at small neck size on the basis of the variational function (20). Notice that, provided a is small, the stationarity conditions $\partial\Phi/\partial R_i = 0$ lead to values for R_1 and R_2 which differ from the solutions $R_\pm(\sigma,p)$ of Eq. (11) only by terms of order a. Thus, near the stationary points, we may replace R_1 and R_2 in Eq. (20) by $R_\pm(\sigma,p)$ to obtain a function $\Phi(a)$ of the neck size a alone. $\Phi(a)$ plays the role of a Landau function in which a is the order parameter. Using Eqs. (11) and (12) to evaluate $C(\sigma,p) = C(\sigma,p,R_A(\sigma,p),R_B(\sigma,p))$

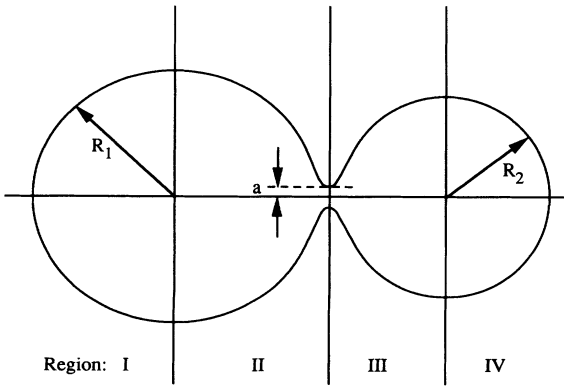

FIG. 3. Toy-model variational shape for two spheres joined by a narrow neck. The outer regions, I and IV, are spherical caps. The inner regions, II and III, are described by the trial function Eq. (13).

and $D(\sigma,p)=D(\sigma,p,R_A(\sigma,p),R_B(\sigma,p))$, we arrive at the Landau function,

$$\Phi_{AB}(a)=\Phi_0(R_A(\sigma,p))+\Phi_0(R_B(\sigma,p)) +4\pi a(1-1/R_A-1/R_B) -D(\sigma,p)\pi a^2\ln a+O(a^2)\ , \tag{23}$$

where R_A and R_B may independently be either one of the two equilibrium sphere radii (12) [35]. Notice (Fig. 4) that, as long a $D(\sigma,p)$ is positive, the Landau function has a boundary minimum whenever $(1/R_A+1/R_B)<1$, so the vesiculated state ($a=0$) is variationally stable to the formation of a small neck. Conversely, when $(1/R_A+1/R_B)>1$, the vesiculated state is variationally unstable to the formation of a small neck. This is just the condition (1) mentioned in the Introduction. For $(1/R_A+1/R_B)\gtrsim 1$, Eq. (23) predicts a small stable neck having a radius given by the solution to [36]

$$(1/R_A+1/R_B-1)=(2\sigma-p)(-a\ln a)+O(a)\ . \tag{24}$$

To proceed further, it is necessary to locate the loci (see Fig. 5) on which the left side of Eq. (24) vanishes. There are three cases.

(a) The quantity $(1/R_+ +1/R_-)$ equals unity along the line $\sigma=\frac{1}{2}$, and Eqs. (12) and (24) predict stable necks in the region just to the right of this line (see Fig. 5) with radii satisfying

$$(\sigma-\tfrac{1}{2})=(p-1)(-a\ln a)\ . \tag{25}$$

(b) $R_+(\sigma,p)=2$ along the line $\sigma=p$ for $\sigma>\frac{1}{2}$, and there are stable small necks in the region just to the left of this line with radii satisfying

$$(p-\sigma)=\frac{p}{2}(2p-1)(-a\ln a)\ . \tag{26}$$

(c) $R_-(\sigma,p)=2$ along the line $\sigma=p$ for $\sigma<\frac{1}{2}$, and there are stable small necks in the region just to the right of this line with radii satisfying

$$(\sigma-p)=\frac{p}{2}(1-2p)(-a\ln a)\ . \tag{27}$$

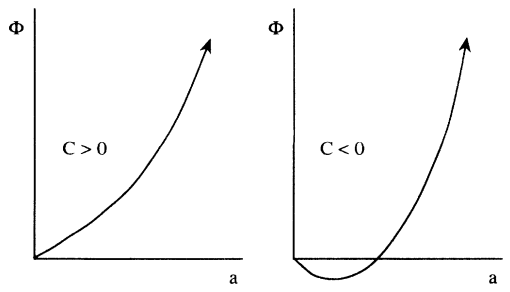

FIG. 4. Characteristic shapes of the Landau function ($D>0$). When $C>0$, the lowest free energy occurs at neck radius $a=0$ and corresponds to a vesiculated shape. When $C<0$, the lowest free energy occurs for $a>0$, corresponding to a necked (budded) shape. The condition $C=0$, which marks the vesiculation boundary, gives the kissing condition, Eq. (1).

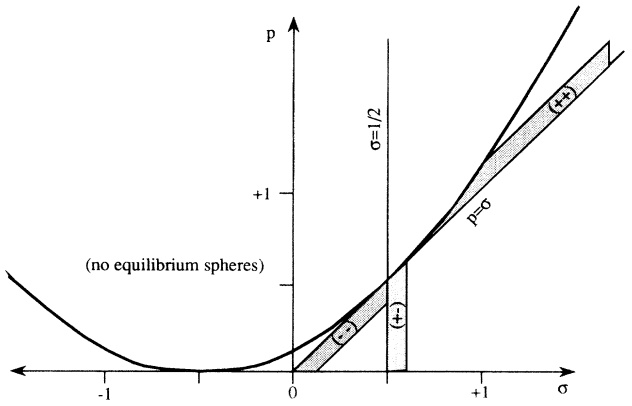

FIG. 5. The (σ,p) plane, showing the vesiculation boundaries for two-sphere osculation and the corresponding regions where small necks occur. Above the parabola $p=(2\sigma+1)^2/8$, there are no stable spherical solutions. Outside this boundary, there are in general two solutions R_+ and R_-, as given by Eq. (12). These two radii are positive when $\sigma>-\frac{1}{2}$ and $p>0$. Within this region, kissing of unequal $(+-)$ spheres occurs along the line $\sigma=\frac{1}{2}$, while equal-sphere $(++)$ and $(--)$ kissing occurs for $\sigma=p$. Shading marks the regions, near these boundaries, where stable necks of small but nonzero radius occur.

A remark is in order concerning the relative mechanical energies of vesiculated and necked shapes in regions where both exist [37]. To compare energies, it is convenient to return to area-volume variables, (A,V). Consider a vesiculated configuration consisting of two spheres of radii R_1 and R_2 with $R_1\neq R_2$, so that $V=4\pi(R_1^3+R_2^3)/3$ and $A=4\pi(R_1^2+R_2^2)$. Suppose that a small neck of radius a is allowed to open up between spheres, so that the overall shape is given by Fig. 3. In this process the radii R_1 and R_2 are allowed to readjust so that A and V remain fixed. Equations (17)–(19) allow calculation of the total mechanical energy as a function of the neck radius,

$$E_{A,V}(a)-E_{A,V}(0)=4\pi a\left[1-\frac{1}{R_1}-\frac{1}{R_2}\right] -2\pi\left[\frac{1}{R_1^2}+\frac{1}{R_2^2}\right]a^2\ln a+O(a^2)\ , \tag{28}$$

which should be compared with Eq. (23). Note that the energy required to make a small neck at fixed (A,V) vanishes with the neck radius [38]. The condition $(1/R_1+1/R_2)\gtrsim 1$ for small stable necks reemerges from this perspective. Mapping back to (σ,p) regenerates Eq. (25). The line of reasoning leading to Eq. (28) cannot be carried through for the symmetric dumbbell $R_1=R_2$, since [39] for this case the neck radius cannot be independently adjusted at fixed A and V. Indeed, it is not possible to reach the line $p=\sigma$ away from the point $p=\sigma=\frac{1}{2}$ except by following a special trajectory in the (A,V) plane.

We shall find in Sec. VI that all the results derived here variationally for the "toy" model, Fig. 3, are, in fact, ex-

act consequences of the Helfrich Eq. (4) for two spheres near the vesiculation boundary. This includes the location of the bifurcation lines [the "kissing condition," Eq. (1)], the condition, $(1/R_1+1/R_2)\gtrsim 1$, for small-neck stability, and the formulas (25)–(27) for the neck radii through order $a\ln a$. (We have checked these relations for a variety of specific examples by numerical integration of the Helfrich equations.) We shall discuss in Sec. VI the reason for this remarkable agreement. Broadly, however, it follows from the fact that Eq. (13) correctly captures the dominant feature of the neck shape when a is small.

IV. PERTURBATIONS ABOUT A SIMPLE CLOSED SHAPE

Suppose $c_m^{(0)}(s)$ and $c_p^{(0)}(s)$, $s\in[0,s_f]$, are solutions of Eqs. (4) and (5) corresponding to a particular closed shape, so that (in the notation of Sec. II) $c_m^{(0)}(s=0)=c_p^{(0)}(s=0)=c_i^*\equiv c_i^*(\sigma,p)$ and $c_m^{(0)}(s=s_f)=c_p^{(0)}(s=s_f)=c_f^*\equiv c_f^*(\sigma,p)$, where c_i^* and c_f^* are the initial and final axial curvatures. For example, in the region of the (σ,p) plane where spheres are mechanically stable, the constant functions,

$$c_m^{(0)}(s)=c_p^{(0)}(s)=1/R(\sigma,p)\ , \tag{29}$$

solve Eqs. (4) and (5), provided that $R(\sigma,p)$ is one of the two special radii (12) [40], so in this case $c_i^*=c_f^*=1/R(\sigma,p)$ and $s_f=\pi R(\sigma,p)$. We now ask, "How is the shape modified if we start the integration with initial curvature $c=c_i^*+\epsilon$, close to but not equal to c_i^*?" To approach this question quantitatively, we may expand about the closed solution,

$$c_{m,p}(s)-c_{m,p}^{(0)}(s)\equiv\delta c_{m,p}(s)=\sum_{n=1}^{\infty}\epsilon^n c_{m,p}^{(n)}(s)\ , \tag{30}$$

substitute into Eqs. (4) and (5), and collect powers of ϵ. The resulting (linear) equations must then be solved, subject to the boundary conditions that the functions $c_{m,p}^{(n)}(s)$ should be regular at $s=0$ with $c_{m,p}^{(1)}(s=0)=1$ and $c_{m,p}^{(n)}(s=0)=0$ for $n>1$, which determine the perturbations uniquely [41]. Since the shapes generated by the Euler equations are smooth except as they approach the axis at $s\to s_f$, $r\to 0$ [42], we anticipate that the deviations will remain small up to the neck region, where they must diverge in order to generate the onduloid/nodoid shapes depicted in Fig. 2.

We illustrate this program explicitly for perturbations about the spherical Euler shapes (29). (The general case will be discussed in Sec. VII.) In this case linearization leads to

$$\left[\frac{d^2}{dr^2}+\frac{(3-2r^2/R^2)}{r(1-r^2/R^2)}\frac{d}{dr}-\frac{(pR^2-2)}{2R(1-r^2/R^2)}\right]c_p^{(1)}(r)=0\ . \tag{31}$$

The substitution $y=r^2/R^2$ reduces Eq. (31) to the hypergeometric equation. Regularity at $r=0$ picks the solution which is a pure hypergeometric function [43], and the unique solution to linear order is

$$\delta c_p(r)=\epsilon F(A,B,2;y)+O(\epsilon^2)\ , \tag{32}$$

where

$$A+B=\tfrac{1}{2}\ ,\qquad AB=\frac{R}{8}(pR^2-2)=\frac{R^2}{8}\left[(2\sigma+1)-\frac{4}{R}\right]\ . \tag{33}$$

This form is only valid on the initial side of the sphere belly (region I in Fig. 3); however, Eq. (32) is regular in the variable s at the belly, and it is straightforward to continue [44] into region II, where the solution is

$$\delta c_p(r)=\frac{\epsilon\pi^{1/2}}{2}\left[\frac{F(A,B,-1/2;1-y)}{\Gamma(2-A)\Gamma(2-B)}-\frac{8}{3}(1-y)^{3/2}\frac{F(2-A,2-B,5/2;1-y)}{\Gamma(A)\Gamma(B)}\right]+O(\epsilon^2)\ . \tag{34}$$

Note that $\delta c_p(r)$ is perfectly finite at the belly of the sphere ($y=1$) but diverges upon approach to the neck ($y\to 0$).

By expanding Eq. (34) near the neck [43], we find

$$c_p(r)=\frac{1}{R}+\epsilon\left[\frac{\alpha R^2}{r^2}+\beta\ln\frac{r}{R}+O(1)\right]+O(\epsilon^2) \tag{35}$$

and, from Eq. (5),

$$c_m(r)=c_p(r)+r\frac{dc_p(r)}{dr}=\frac{1}{R}+\epsilon\left[-\frac{\alpha R^2}{r^2}+\beta\ln\frac{r}{R}+O(1)\right]+O(\epsilon^2)\ , \tag{36}$$

where

$$\alpha=-\frac{2\sin(\pi A)\sin(\pi B)}{\pi(1-A)(1-B)}\ ,\qquad \beta=-\frac{4\sin(\pi A)\sin(\pi B)}{\pi}\ , \tag{37}$$

with

$$\sin(\pi A)\sin(\pi B)=-\frac{1}{2}\cos\left[\frac{\pi}{2}(1+4R-2pR^3)^{1/2}\right]\ ,\qquad (1-A)(1-B)=\tfrac{1}{8}(pR^3-2R+4)\ , \tag{38}$$

from Eq. (33). Equations (35) and (36) should be a good representation near but not too near the neck, i.e., $\epsilon\alpha R^3\ll r^2\ll R^2$, so that the perturbation remains small. Note that, for r in this interval, successive terms in Eqs. (35) and (36) are decreasing in magnitude. We shall need these results in Secs. VI and VII.

V. SCALING NEAR A NARROW NECK

Solution of the shape equations (4) and (5) in the vicinity of a very narrow neck of radius a is simplified by using the scaled variables, $\rho=r/a$, $P(\rho)=ac_p(r)$, and

$\Psi(\rho)=a[c_p(r)+c_m(r)]$, in terms of which the Helfrich equations (4) and (5) become

$$\frac{d\Psi}{d\rho}=\frac{\rho}{2(1-\rho^2P^2)} \times\{P[\Psi(2P-\Psi)-2aP+a^2]+2\sigma a^2P-pa^3\}\ , \qquad \frac{dP}{d\rho}=\frac{\Psi-2P}{\rho}\ . \tag{39}$$

The boundary conditions which characterize a neck of radius a are $P(1)=1$ and $\Psi(1)=1-a/b(a)=a-\sigma a^2+O(a^3)$ (which are *not* independent), as outlined in the Appendix, Eqs. (A3)–(A5). A second integration constant remains free and sets the asymmetry of the neck, as discussed in the Appendix.

When $a\to 0$, these equations (and boundary conditions) admit the solution $\Psi(\rho)=0, P(\rho)=1/\rho^2$. Note that $\Psi(1)\to 0$ in this limit, so this behavior is generic. It is significant that the specific parameters p and σ drop out, so the shape in the neck region is universal. Ψ is the mean curvature, and its vanishing means that the scaled neck shape is a so-called minimal surface [45] in the limit $a\to 0$. Corrections to this shape may now be computed systematically by inserting the ansatz

$$\Psi(\rho)=\sum_{n=1} a^n\Psi_n(\rho)\ , \qquad P(\rho)=\frac{1}{\rho^2}+\sum_{n=1} a^nP_n(\rho) \tag{40}$$

into Eqs. (39). This procedure generates a sequence of linear inhomogeneous differential equations, corresponding to successive powers of a,

$$\frac{d\Psi_n}{d\rho}=\frac{\Psi_n}{\rho(\rho^2-1)}+Q_n(\{P_m,\Psi_m;m<n\};\rho)\ , \qquad \frac{dP_n}{d\rho}=-\frac{2P_n}{\rho}+\frac{\Psi_n}{\rho}\ ,\quad n=0,1,2,3,\ldots\ . \tag{41}$$

The procedure is recursive in that the function $Q_n(\{P_m,\Psi_m;m<n\};\rho)$ involves solutions from all levels lower than n. Because the equations are first order, all solutions can be reduced to quadratures, and the formal solutions are

$$\Psi(\rho)=\frac{(\rho^2-1)^{1/2}}{\rho}\sum_{n=1} a^n\left[K_n+\int^\rho dy\frac{yQ_n(y)}{(y^2-1)^{1/2}}\right] \tag{42}$$

and

$$P(\rho)=\frac{1}{\rho^2}\left[1+\sum_{n=1} a^n\int_1^\rho dy\, y\Psi_n(y)\right]\ . \tag{43}$$

Note that the integrals in Eq. (43) are definite, while those in Eq. (42) are indefinite, since (as we shall find) divergences may appear both at $\rho\to 1$ and at $\rho\to\infty$. The parameters K_n are constants of integration and are collectively equivalent [46] to the asymmetry parameter g (see Appendix).

Equations (42) and (43) already contain the boundary conditions which define the neck radius. This occurs explicitly for $P(\rho)$, since the integrals are regular [47] at $\rho=1$ and only the leading term contributes to $P(1)$. The situation for $\Psi(\rho)$ is more subtle: At each order [47], the integrated term diverges at $\rho\to 1$ in just such a way as to cancel the factor $(\rho^2-1)^{1/2}$ and give a finite contribution to $\Psi(1)$. These finite contributions are independent of the integration constants K_n and build up order by order in a the initial value computed in the Appendix.

It is a straightforward exercise to generate the first few iterates in the hierarchy (40). We find

$$\Psi_1(\rho)=1+K_1\frac{\sqrt{\rho^2-1}}{\rho}\ , \tag{44}$$

$$P_1(\rho)=\frac{1}{2}\left[1-\frac{1}{\rho^2}\right]+\frac{K_1}{2\rho^2}[\rho\sqrt{\rho^2-1}-\ln(\rho+\sqrt{\rho^2-1})]\ , \tag{45}$$

and

$$\Psi_2(\rho)=K_2\frac{\sqrt{\rho^2-1}}{\rho}-\frac{K_1^2}{2}\left[1-\frac{\rho}{\sqrt{\rho^2-1}}\ln(\rho+\sqrt{\rho^2-1})\right]-\sigma\left[1-\frac{\sqrt{\rho^2-1}}{\rho}\ln(\rho+\sqrt{\rho^2-1})\right]\ . \tag{46}$$

$P_2(\rho)$ can be obtained from (46) by the integration (43). It is then straightforward to evaluate $\Psi(\rho)$ and $P(\rho)$ for small a and $\rho\gg 1$:

$$\Psi(\rho)=a(1+K_1)+a^2\left[K_2+\left[\frac{1}{2}K_1^2+\sigma\right](\ln 2-1)\right]+a^2\left[\frac{1}{2}K_1^2+\sigma\right]\ln\rho+aO\left[\frac{1}{\rho^2}\right]+a^2O\left[\frac{\ln\rho}{\rho^2}\right]+O(a^3) \tag{47}$$

and

$$P(\rho)=\frac{a}{2}(1+K_1)+\frac{1}{\rho^2}-\frac{aK_1}{2\rho^2}\ln\rho+\frac{a^2}{2}\left[\frac{1}{2}K_1^2+\sigma\right]\ln\rho+aO\left[\frac{1}{\rho^2}\right]+a^2O(1)+O(a^3)\ . \tag{48}$$

VI. MATCHING AND THE KISSING CONDITION FOR SPHERES

The small neck of Sec. IV, caused by an "error" ϵ in the initial axial curvature, can, of course, be described as a scaling shape in the sense of Sec. V in terms of the two parameters a and g. In this sense, then, there must be unique dependences $a(\epsilon)$ and $g(\epsilon)$. When ϵ is small (and, therefore, a is small) this dependence can be read off by matching the coefficients of the leading terms of, for example, Eqs. (35) and (48) in the asymptotic region, $\epsilon\alpha R^3\ll r^2\ll R^2$. This matching gives [48]

$$\frac{1}{R}=\frac{1}{2}(1+K_1)-\frac{1}{2}\left[\frac{1}{2}K_1^2+\sigma\right]a\ln a+O(a^2) \quad (49)$$

for the leading (constant) term,

$$\epsilon\alpha R^2=a\left[1+\frac{aK_1}{2}\ln a+O(a)\right] \quad (50)$$

for the $1/r^2$ term, and

$$\epsilon\beta=\frac{a}{2}\left[\frac{1}{2}K_1^2+\sigma\right]\left[1+\frac{aK_1}{2}\ln a+O(a)\right] \quad (51)$$

for the coefficient [49] of $\ln r$.

The first of these equations shows that K_1 depends on the sphere radius R but is independent of ϵ at leading order. Equivalently, it may be regarded as giving the leading behavior of the asymmetry parameter (Appendix) [46],

$$g(\epsilon)=\frac{a(\epsilon)}{3}\left[\frac{2}{a(\epsilon)}\right]^{3/2}\left[\frac{2}{R}-1\right], \quad (52)$$

showing that g diverges as $\sqrt{a}$ as $a\to 0$, unless $R=2$, as occurs for symmetric coexistence. Equation (50) shows that the neck radius scales linearly with ϵ as $\epsilon\to 0$ with a coefficient which can be calculated from Eqs. (37) and (38) and may have either sign (depending on σ and p). Equation (51) can be shown equivalent to Eq. (50) by using the relations (37) and (38). A similar comparison of Eq. (47) with the perturbation result for Ψ at leading orders (constant and logarithmic) turns out to give redundant information. Note that, in the region of the match, the omitted terms in Eqs. (47) and (48) are, indeed, smaller than those that contribute to the matching. The dominant corrections to the leading behavior are of relative order $a\ln a$. Further corrections are of order a and higher. Higher-order terms, $c_{m,p}^{(n)}(r)$, $\Psi_n(\rho)$, and $P_n(\rho)$, would presumably allow one to infer additional contributions to the functions $a(\epsilon)$ and $g(\epsilon)$.

The kissing condition (1) for spherical multiplets follows immediately from Eq. (49). Referring to Fig. 3, suppose that integration from the left leads to a small neck of radius $a\to 0$, so $1/R_1=(1+K_1)/2$. The sign of the asymmetry parameter changes across the neck (Appendix), so on the right side $1/R_2=(1-K_1)/2$. In adding these equations, the asymmetry parameter cancels out and we are led to the kissing condition. As explained in Sec. III, this condition is satisfied for spheres along the two special lines $\sigma=\frac{1}{2}$ and $\sigma=p$. Finally, when a is small but not zero, we keep the $a\ln a$ terms in Eq. (49) and are led directly to Eq. (24) for the radius of the small neck, from which Eqs. (25)–(27) of the toy model are derived, finally now on a firm basis.

This exact agreement with the toy-model results may seem surprising. In order to understand its origin, it is useful to study directly the behavior of the free energy (3) near the kissing boundary in order to derive the a and $a\ln a$ terms in Eq. (23) on the basis of the solutions we have now developed for the full Helfrich equations. Consider a point (σ,p) near one of the kissing boundaries [Eqs. (25)–(27)]. We wish to calculate the free-energy difference between the free energies of the exact Euler shape [described by the function $c_p(r)$] and the corresponding multiplet of coexisting spheres [cf., Eq. (23)]. This difference may be evaluated as

$$\begin{aligned}\Delta\Phi_{AB}(\sigma,p)&\equiv\Phi[c_p]-\Phi_0(R_A(\sigma,p))-\Phi_0(R_B(\sigma,p))\\&=\Phi[c_p]-\Phi[c_p-\delta c_p]\,,\end{aligned} \quad (53)$$

where δc_p is defined by (30) with the value of ϵ appropriate to the Euler shape at (σ,p). If the perturbation δc_p were always small, then the variational property of the Euler shape would guarantee that $\Delta\Phi_{AB}$ is of order ϵ^2 (i.e., of order a^2), smaller than the terms in Eq. (23), which are of order $a^2\ln a$. Thus, through this order, the entire contribution to the exactly calculated $\Delta\Phi_{AB}$ must come from the neck region, where the perturbation is not small (since $c_p\to\infty$ at the neck for the fully vesiculated shape). To calculate $\Delta\Phi_{AB}$ in this region, we use the scaling representation (40). A direct but messy calculation using Eq. (45) leads to Eq. (23), thus showing that the toy-model results are, indeed, exact up through order $a^2\ln a$. Furthermore, in doing the calculation, one finds that the only terms in $P(\rho)$ which contribute at this order are the leading terms at large ρ, i.e., $P(\rho)=a/R+1/\rho^2$, which are duplicated (for small a) by the toy-model ansatz (13). Thus, near the kissing boundary, the toy-model results are all correct because the trial function (13) captures the key part of the singular behavior near the neck.

VII. THE KISSING CONDITION FOR GENERAL AXISYMMETRIC OSCULATING SHAPES

It is natural to ask whether the kissing condition (1) always remains valid for axisymmetric but nonspherical shapes, as has been observed numerically in a few cases [1,3]. The result of the preceding section suggest strongly that this is the case, since we have found that it is only the behavior near the narrow neck (i.e., for $r\ll R$) which contributes to the kissing condition and the nearby scaling behavior. We sketch below [50] how to extend the matching analysis of Sec. VI to nonspherical shapes. The upshot of this more general analysis is that the form of the a dependence is unchanged. The kissing condition remains valid, where R_1 and R_2 now refer to the local radii of curvature on the two sides of the (narrow) neck. Equation (24) for the scaling of the neck radius continues to hold, only with a coefficient which is no longer $(2\sigma-p)$.

The key point is the generalization of the perturbation analysis [see Eq. (30) and what follows] when the closed shape described by $c_{m,p}^{(0)}(r)$ is not simply spherical, as in Eq. (29). In place of Eq. (31), linearization now leads to an equation of the form

$$\left[\frac{d^2}{dr^2}+\frac{Q(r)}{r}\frac{d}{dr}-T(r)\right]c_p^{(1)}(r)=0\,, \quad (54)$$

where the coefficients $Q(r)$ and $T(r)$ depend on the functions $c_{m,p}^{(0)}(r)$ and have the following important properties.

(a) They depend only on the variable r^2 [51].

(b) They go to constant values as $r \to 0$, so Eq. (54) has a singular point at $r=0$.

(c) $Q(0)=3$.

Specifically, a short calculation shows that, near $r=0$,

$$Q(r)=Q_0+Q_2r^2+\cdots=3+r^2/R^2+O(r^4) \tag{55}$$

and

$$T(r)=T_0+T_2r^2+\cdots=\frac{1}{2}\left[(2\sigma+1)-\frac{4}{R}\right]+O(r^2)\ , \tag{56}$$

where $1/R$ is henceforth the local curvature $c_p^{(0)}=c_m^{(0)}$ evaluated at the axis. A simple analysis [52] close to the singularity shows that the two independent solutions of Eq. (54) have the forms

$$f^{(1)}(r)=1+\frac{T_0}{8}r^2+O(r^4)+\cdots\ , \tag{57}$$

which is regular and describes a perturbation which makes a (small) change in the initial (axial) curvature, and

$$f^{(2)}(r)=\frac{1}{r^2}[1+O(r^2)+\cdots]+\left[\frac{T_0}{2}+\frac{1}{R^2}+O(r^2)\right]\ln r\ , \tag{58}$$

which is singular and describes a (small) neck. Now, this is precisely the form of Eq. (35), and one verifies immediately that, for spheres, $\beta/\alpha R^2$ agrees with the coefficient $\gamma \equiv T_0/2+1/R^2$ of the logarithm in Eq. (58). Note that, just as for spheres, the perturbative form (58) is valid far from the neck ($r \gg a$), so that perturbation theory still holds, but still near the axis ($r \ll R$), so that neglect of higher powers of r^2 near the singular point remains justified [53].

At this point the analysis of Sec. VI can be repeated: The general perturbative solution has leading singular behavior [54]

$$c_p(r)=\frac{1}{R}+C\left[\frac{1}{r^2}+\gamma\ln r\right]\ , \tag{59}$$

where C is an unknown integration constant. This must be matched to the scaling form (48). Equations (49)–(51) reemerge, only with $\epsilon\alpha R^2$ now replaced by the integration constant C. The upshot is that the kissing condition (1) is satisfied with respect to the local axial radii of curvature at the osculation point, while near but not at the kissing boundary the radius of the neck is given by

$$\left[\frac{1}{R_1}+\frac{1}{R_2}-1\right]=\left[\frac{1}{2}\left[\frac{2}{R}-1\right]^2+\sigma\right]\times(-a\ln a)+O(a)\ , \tag{60}$$

where R on the right is either one of the two coexisting axial radii of curvature, R_1 and R_2. This expression generalizes Eq. (24) to nonspherical shapes.

What forms do necks take for nonaxisymemtric shapes? When two nearby buds are produced from the same parent vesicle, do the necks attract or repel? What is the dynamics of bud formation? These and many other related questions remain open.

ACKNOWLEDGMENTS

We are grateful to Evan Evans for introducing us to budding phenomena, so beautifully observed in his lab. We thank U. Seifert for many useful discussions. This work was funded in part by the National Science and Engineering Research Council of Canada and by the U.S. National Science Foundation through the Division of Materials Research.

APPENDIX: BEHAVIOR OF EULER SHAPES NEAR NECK AND BELLY POINTS

Near extremal points of the radius, the analyticity of the Euler shapes may be expressed by writing

$$t^2 \equiv |r(s)-a| = a_2s^2+a_3s^3+\cdots\ , \tag{A1}$$

where $r(s)$ is the radius from the symmetry axis, a is the extremal radius, $t \equiv +\sqrt{|r-a|}$, and the arc length s is measured from the extremal point. Since the left side of Eq. (A1) depends only on t^2, inversion expresses $s(r)$ in the form

$$s(r)=\pm b_1t+b_2t^2\pm b_3t^3+b_4t^4\pm\cdots\ , \tag{A2}$$

where the upper (lower) sign refers to the positive, near-side (negative, far-side) branch, i.e., analyticity requires that all odd-power terms change sign across the extremum. It is then a consequence of Eqs. (6)–(9) that the same is true of the curvatures $c_m(r)$ and $c_p(r)$. We have made use of this in deriving the continuation (34).

Coefficients in expansions like (A1) and (A2) are, of course, constrained by the shape equations in such a way that each neck (or belly) is characterized by two parameters, corresponding to the integration constants of the two first-order equations (4) and (5). One of these parameters is the extremal radius. We illustrate the structure in connection with the behavior of the curvatures near a neck of radius a (the corresponding belly solution differs by a few sign changes):

$$c_p(r)=\sum_{n=0}^{\infty}p_nt^n=\frac{1}{a}-\frac{1}{a}\left[\frac{1}{a}+\frac{1}{b}\right]t^2+\frac{g}{a}t^3+\cdots \tag{A3}$$

and

$$c_m(r)=\sum_{n=0}^{\infty}m_nt^n=-\frac{1}{b}+\frac{3}{2}gt+\cdots\ . \tag{A4}$$

The initial value of c_m at the neck is fixed by the singular structure of Eq. (4),

$$c_m(a)=m_0(a)=-\frac{1}{b(a)}=-\left[\left[\frac{1}{a}-1\right]^2+(2\sigma-ap)\right]^{1/2}\ . \tag{A5}$$

The parameter g is not fixed by the equations and may be regarded as the second integration constant. The remain-

ing coefficients beyond those shown explicitly in Eqs. (A3) and (A4) are functions of the two integration constants a and g. In particular, both $p_n(a,g)$ and $m_n(a,g)$ depend polynomially on the parameter g. For even n, the polynomial is even. For odd n the polynomial is odd, so odd coefficients vanish at $g=0$. When $g=0$, the neck is symmetric. When $g\neq 0$, the neck is asymmetric and the sign of g changes from one side of the neck to the other in accordance with the analyticity property. We shall refer to g as the asymmetry parameter.

[1] L. Miao, B. Fourcade, M. Rao, M. Wortis, and R. K. P. Zia, Phys. Rev. A **43**, 6843 (1991).

[2] J. C. Luke and J. I. Kaplan, Biophys. J. **25**, 107 (1979).

[3] U. Seifert, K. Berndl, and R. Lipowsky, Phys. Rev. A **44**, 1182 (1991). See also K. Berndl, J. Käs, R. Lipowsky, E. Sackmann, and U. Seifert, Europhys. Lett. **13**, 659 (1990).

[4] S. Svetina and B. Žekš, Biomed. Biochim. Acta **42**, S86 (1983); **44**, 979 (1985); Euro. Biophys. J. **17**, 101 (1989).

[5] W. Wiese and W. Helfrich, J. Phys. Condens. Matter **2**, SA329 (1990).

[6] W. Wiese, W. Harbich, and W. Helfrich, J. Phys. Condens. Matter **4**, 1647 (1992).

[7] E. Sackmann, H. P. Duwe, and H. Engelhardt, Faraday Discuss. Chem. Soc. **81**, 281 (1986).

[8] E. Evans and W. Rawicz, Phys. Rev. Lett. **64**, 2094 (1990).

[9] J. Käs and E. Sackmann, Biophys. J. **60**, 825 (1991).

[10] J. Käs, E. Sackmann, S. Svetina, and B. Žekš, J. Phys. (Paris) II **3**, 631 (1993).

[11] Physically, of course, there is always a short-distance cutoff (e.g., the membrane thickness), below which new physics enters the problem and prescribes a well-defined configuration for the "infinitesimal" neck. Such a "microscopic" description requires going beyond the Helfrich model, Eq. (2).

[12] In a pitchfork bifurcation, the central minimum of the Landau function becomes unstable at the transition and two new stable minima appear at nonzero order parameter. For us, the point $a=0$ is a "boundary" point in the space of configurations, where the free energy is either a local maximum or a local minimum but the shape does not satisfy Euler equations, except at the transition. Thus, technically, what happens is that on one side there are no (nearby) solutions of the Euler equations. A solution first appears (at the transition) at the boundary point and immediately bifurcates away to nonzero values of the order parameter. Except for the logarithmic factor, this is much like a "transcritical" bifurcation (only with the $\varphi=0$ state missing). See J. Guckenheimer and P. Holmes, *Nonlinear Oscillations, Dynamical Systems, and Bifurcations of Vector Fields* (Springer-Verlag, New York, 1983), p. 145 ff.

[13] In particular, in the notation of Eqs. (3)–(5), $\sigma=\frac{1}{2}$, $p\leq\frac{1}{2}$ is the kissing boundary for spheres of unequal radius, while $\sigma=p$ corresponds to coexisting Helfrich spheres and marks the boundary for equal-sphere kissing.

[14] W. Helfrich, Z. Naturforsch., Teil C **28**, 693 (1973).

[15] H. J. Deuling and W. Helfrich, J. Phys. (Paris) **37**, 1335 (1976).

[16] M. P. Sheetz and S. J. Singer, Proc. Natl. Acad. Sci. U.S.A. **71**, 4457 (1974).

[17] E. Evans, Biophys. J. **14**, 923 (1974); **30**, 265 (1980).

[18] W. Helfrich, Z. Naturforsch, Teil C **29**, 510 (1974).

[19] S. Svetina, A. Ottova-Lietmannová, and R. Glaser, J. Theor. Biol. **94**, 13 (1982).

[20] S. Svetina, M. Brumen, and B. Žekš, Stud. Biophys. **110**, 177 (1985).

[21] U. Seifert, L. Miao, H.-G. Döbereiner, and M. Wortis, in *Structure and Conformation of Amphiphilic Membranes*, edited by R. Lipowsky, D. Richter, and K. Kremer (Springer, Berlin, 1992), pp. 93–96.

[22] V. Heinrich, S. Svetina, and B. Žekš, Phys. Rev. E **48**, 3112 (1993).

[23] L. Miao, U. Seifert, M. Wortis, and H.-G. Döbereiner, Phys. Rev. E **49**, 5389 (1994).

[24] J. Kevorkian and J. D. Cole, *Perturbation Methods in Applied Mathematics* (Springer-Verlag, New York, 1981).

[25] P. B. Canham, J. Theor. Biol. **26**, 61 (1970).

[26] σ and p are, respectively, the mechanical surface tension and the pressure difference between the inside and outside of the vesicle.

[27] Axisymmetric solutions are at mechanical equilibrium; however, all mechanically equilibrated solutions are not axisymmetric. Lowest-energy states are often but not always axisymmetric. See Refs. [3,22] and also M. A. Peterson, J. Appl. Phys. **57**, 1739 (1985); U. Seifert, J. Phys. A **24**, L573 (1991); Phys. Rev. Lett. **66**, 2404 (1991).

[28] It is a consequence of Eq. (5) that the condition for the shape to be smooth at the axis is $c_m=c_p$, whenever $r\rightarrow 0$.

[29] Even if self-intersecting surfaces were accepted, the assignment of a volume to Fig. 2(c) would be ambiguous.

[30] Note that, from this perspective, the kissing boundary marks a "level crossing" between one closure value $c_i^{*(s)}(\sigma,p)$, corresponding to a single compact closed shape, and another, $c_i^{*(n)}(\sigma,p)$, corresponding to a necked shape.

[31] Figure 3 is drawn for a "dumbbell" configuration, corresponding to exterior vesiculation. It is quite possible to describe interior vesiculation, in which one sphere encloses the other, in a similar way. To do this would require taking one of the radii $R_{1,2}$ positive and the other negative. In what follows we shall assume for definiteness that R_1 and R_2 are both positive.

[32] In forming the trial function (13) we have matched to the spherical caps at $\Theta=\pi/2$. In fact, it is not hard to show that the results below for the singular behavior are insensitive to the angle at which the matching is done. The reason is that, when the neck is small, all the singular behavior comes from the neck region.

[33] The smoothness of the match suffices to prevent any boundary contributions to the free-energy functional.

[34] I. S. Gradshteyn and I. M. Ryzhik, *Tables of Integrals, Series, and Products* (Academic, New York, 1965). See Formulas 8.111–8.114.

[35] The common case of asymmetric (i.e., unequal, spherical) buds corresponds to $(AB)=(+-)$. The choices $(++)$ and $(--)$ correspond to the vesiculation from symmetric (spherical) dumbbells. Each has its own characteristic locus in the (σ,p) plane, as we shall see below.

[36] $(2\sigma-p)$ is always positive in the regions of interest.

[37] Note that "stability" in the preceding paragraph refers to the free energy Φ, not the mechanical energy E.

[38] Since the trial function of Fig. 3 is variational, any exactly computed minimum-energy shape with the same area and volume can only have lower energy. Thus Eq. (28) provides an upper bound to the neck energy in any region where the vesiculated shape is stable.

[39] Of course, it is possible to open a neck and simultaneously to allow the symmetry to be broken. This is just the limiting case of Eq. (28), as $R_1 \rightarrow R_2$, and one finds stable necks for $2/R \gtrsim 1$ with $(2/R-1)=(\frac{1}{4})(-a \ln a)$, corresponding to Eq. (25) at $p=\sigma=\frac{1}{2}$.

[40] It is easy to verify that the radii of curvature (12) make the curly bracket on the right of Eq. (4) vanish.

[41] The perturbations $c_{m,p}^{(n)}(s)$ satisfy second-order linear inhomogeneous equations with one solution which is singular at $s=0$.

[42] Singularities are generated in the r variable whenever the denominator on the right side of Eq. (4) vanishes. This happens at local maxima ("belly points") and local minima ("neck points") of the radius. The overall vesicle shape is not singular at such points, and there is a natural continuation through the "apparent" singularity. See the Appendix.

[43] *Handbook of Mathematical Functions,* edited by M. Abramowitz and I. S. Stegun (Dover, New York, 1972), formulas 15.5.1, 15.5.18,and 15.5.19. See also the transformation formula 15.3.6 and the asymptotic formula 15.3.12.

[44] We have made use of the transformation formula of Ref. [43] and the analytic continuation of our Appendix. Note that $(1-y)^{1/2} \sim t$, while $F(1-y)$ contains only even powers of t. Thus analytic continuation merely changes the sign of the second term in the square brackets of Eq. (34).

[45] J. Almgren, *Plateau's Problem* (Benjamin, New York, 1968). T. J. Willmore, *Total Curvature in Riemannian Geometry* (Ellis Horwood, Chichester, 1982).

[46] It may seem surprising that an infinite number of integration constants appear in Eq. (42) despite the fact that the neck radius has already been fixed, so (as outlined in the Appendix) it takes only a single additional parameter (the asymmetry parameter g) to specify the complete solution. A brief calculation shows that $g=\frac{1}{3}(2/a)^{3/2}\sum_{n=1} a^n K_n$. It is easy to verify that the series solutions, Eqs. (A3) and (A4), can be regenerated term by term from the scaling equations (39). Thus, by construction, the form of the solution generated by Eqs. (42) and (43) can depend only on the parameter g and not on the individual values of the separate K_n's.

[47] This statement can be verified at low order, but we do not have a general proof.

[48] The matching below is done in terms of the variable r belonging to the perturbative solutions. All matching could equally well be done in terms of the variable ρ belonging to the scaling solutions. In this latter form, the logarithmic correction to the $1/R$ formula (49) would come from the $\ln r$ in $c_p^{(1)}(r)$ and the logarithmic corrections to (49) and (51) would arise from terms in $c_p^{(2)}(r)$ and, indeed, allow one to infer contributions to $c_p^{(2)}$ of the forms $\ln r/r^2$ and $(\ln r)^2$, respectively.

[49] The $a \ln a$ correction to the coefficient of $1/r^2$ comes from the $\ln\rho/\rho^2$ term in $P_1(\rho)$. The corresponding (and equivalent) correction to the coefficient of $\ln r$ comes from a term in $P_3(\rho)$ which goes as $(\ln\rho)^2$ at large ρ. There is a corresponding $(\ln\rho)^2$ term in $\Psi_3(\rho)$, which, in turn, arises from a contribution to $Q_3(\rho)$ which varies as $(\ln\rho/\rho)^2$ at large ρ. The calculations are straightforward but messy.

[50] L. Miao, Ph.D. thesis, Simon Fraser University, 1993 (unpublished).

[51] The key point here is that $c_{m,p}^{(0)}(r)$ are even functions of r, as can easily be verified by expanding near the axial caps.

[52] P. M. Morse and H. Feshbach, *Mathematics for Theoretical Physics* (Academic, New York, 1965), formulas 8.111–8.114.

[53] We assume that the shape $c_{m,p}^{(0)}$ is smooth and does not, itself, have sharp curvature near the axis.

[54] At first sight, one may worry that the regular solution (which must in general enter in linear combination with the singular solution) will change the constant term and modify the kissing condition. Direct comparison shows, however, that the coefficient of the singular solution must be $O(a)$ in order to fit the $1/r^2$ and logarithmic terms. Generically, the two coefficients must be the same in magnitude, since their ratio is determined by integrating the full perturbation equation (which contains no small parameters) from the closed end. Thus the coefficient of the regular solution is also small, and its contribution enters only at orders higher than those considered here.

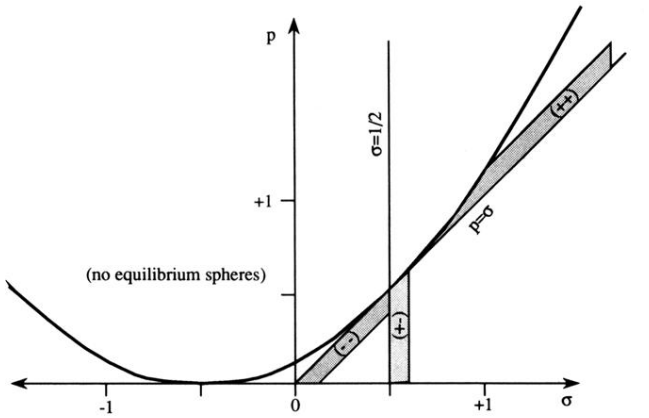

FIG. 5. The (σ,p) plane, showing the vesiculation boundaries for two-sphere osculation and the corresponding regions where small necks occur. Above the parabola $p=(2\sigma+1)^2/8$, there are no stable spherical solutions. Outside this boundary, there are in general two solutions R_+ and R_-, as given by Eq. (12). These two radii are positive when $\sigma > -\frac{1}{2}$ and $p > 0$. Within this region, kissing of unequal $(+-)$ spheres occurs along the line $\sigma=\frac{1}{2}$, while equal-sphere $(++)$ and $(--)$ kissing occurs for $\sigma=p$. Shading marks the regions, near these boundaries, where stable necks of small but nonzero radius occur.